Chinese Journal of Chemical Engineering 42 (2022) 35–41

Contents lists available at ScienceDirect

Chinese Journal of Chemical Engineering

journal homepage: www.elsevier.com/locate/CJChE

Full Length Article

Stable titanium metal–organic framework with strong binding affinity for ethane removal

Puxu Liu [1], Yong Wang [1], Yang Chen [1], Xiaoqing Wang [1], Jiangfeng Yang [1], Libo Li [1,2,*], Jinping Li [1]

[1] College of Chemistry and Chemical Engineering, Shanxi Key Laboratory of Gas Energy Efficient and Clean Utilization, Taiyuan University of Technology, Taiyuan 030024, China
[2] Key Laboratory of Coal Science and Technology, Taiyuan University of Technology, Taiyuan 030024, China

ARTICLE INFO

Article history:
Received 1 April 2021
Received in revised form 19 July 2021
Accepted 19 July 2021
Available online 24 August 2021

Keywords:
Titanium metal-organic framework
Adsorption
Separation
Ethylene purification
Strong binding affinity
Molecular simulation

ABSTRACT

Direct separation of high purity ethylene (C_2H_4) from an ethane (C_2H_6)/ethylene mixture is a critical and challenging task owing to the very similar molecular size and physical properties of the two components. While some studies have attempted this separation, there is a lack of excellent porous materials with strong binding affinity for C_2H_6-selective adsorption *via* an energy-efficient adsorptive separation process. Herein, we report a titanium metal-organic framework with strong binding affinity and excellent stability for the highly efficient removal of C_2H_6 from C_2H_6/C_2H_4 mixtures. Single component adsorption isotherms demonstrated a larger amount of adsorbed ethane (1.16 mmol·g^{-1} under 1 kPa) and high C_2H_6/C_2H_4 selectivity (2.7) for equimolar C_2H_6/C_2H_4 mixtures, especially in the low-pressure range, which is further confirmed by the results of grand canonical Monte Carlo simulations for C_2H_6 adsorption in this framework. The experimental breakthrough curves showed that C_2H_4 with a high purity was collected directly from both 1:9 and 1:15 C_2H_6/C_2H_4 (volume ratio) mixtures at 298 K and 100 kPa. Moreover, the unchanged adsorption and separation performance after cycling experiments confirmed the promising applicability of this material in future.

1. Introduction

Ethylene (C_2H_4) is the main raw material for manufacturing a variety of chemicals, such as polyethylene and ethylene glycol [1,2], and it is produced by methods such as catalytic cracking and dehydrogenation of ethane [3–5]. To meet the criterion of poly grade C_2H_4 (>99.95%), the inevitable byproduct ethane (C_2H_6) obtained during ethylene separation needs to be removed [6–8]. However, the similar physical properties and molecular size of these two components (C_2H_6: $(3.81\times10^{-10})\times(4.08\times10^{-10})\times(4.82\times10^{-10})$ m^3; C_2H_4 $(3.28\times10^{-10})\times(4.18\times10^{-10})\times(4.84\times10^{-10})$ m^3) make their separation quite a challenging task [9–17]. The efficient separation of these two compounds is regarded as one of the seven chemical separations that will have significant global impact [18].

Nowadays, the separation of C_2H_6 and C_2H_4 is still performed mostly by employing conventional cryogenic distillation, operated at a low temperature and high pressure over 100 trays, which accounts for nearly half of the energy consumption in the entire chemical separation process [18]. Thus, the development of a portable and energy-efficient method to separate these homologues is urgently needed [7,19]. Therefore, adsorption separation using porous materials has been developed and has become a focus by many researchers due to advantages such as facile operation requirements and low energy consumption [19–29].

For C_2H_6/C_2H_4 separation, the conventional adsorbents were almost C_2H_4-selective adsorbents due to the π-complexation between the open metal sites (OMS) with the unsaturated olefin. High purity C_2H_4 could only be obtained by regenerating the C_2H_4-selective adsorbents to collect the desire product after multiple adsorption and desorption cycles. It thus would be more portable to fabricate C_2H_6-selective adsorbents straightforwardly in views of a little impurity C_2H_6 in the mixture during the real applications. Because energy consumption and operation cost will be reduced substantially [30–35]. Generally, the mechanisms for preferential C_2H_6 adsorption include the gate-opening effect, the hydrogen-binding affinity, and the difference in the van der Waals force between the framework and gas molecules. The first reported C_2H_6 adsorption material was a type of zeolitic imidazolate framework (ZIF), synthesized by Gascon *et al.* in 2010 [36]. They confirmed that the microporous material ZIF-7 could efficiently and

* Corresponding author at: College of Chemistry and Chemical Engineering, Shanxi Key Laboratory of Gas Energy Efficient and Clean Utilization, Taiyuan University of Technology, Taiyuan 030024, China.
E-mail address: lilibo908@hotmail.com (L. Li).

https://doi.org/10.1016/j.cjche.2021.07.027
1004-9541/

selectively adsorb C_2H_6 over C_2H_4 through the gate-opening effect at a low pressure, but it exhibited a poor separation performance at ambient conditions. Thereafter, in 2015, Chen *et al.* [8] created a microporous metal-organic framework (MOF), MAF-49, that exhibited 1D zigzag channels decorated with a high density of polar nitrogen atoms with the diameter of about 0.3×10^{-9} m, it preferentially captured C_2H_6 *via* multiple hydrogen bonding and electrostatic interactions resulting from its special structure. However, the limited space in this microporous material resulted in a low C_2H_6 adsorption capacity. Subsequently, Li *et al.* [37,38] conducted adsorption and dynamic breakthrough experiments on Ni(bdc)$(ted)_{0.5}$ and PCN-250; they revealed that the unique pore environment and the van der Waals force might account for the large amount of adsorbed C_2H_6. In 2018, Chen *et al.* [39] reported improved C_2H_6/C_2H_4 separation performance by using a microporous MOF $Cu(Qc)_2$; they demonstrated that the optimized pore structure in $Cu(Qc)_2$ could maximize the number of weak host-guest interactions within the MOF, so that the C_2H_6 molecules were well-accommodated in the suitable pores, resulting in improved C_2H_6 adsorption. Further, recently, our group reported the benchmark material $Fe_2(O_2)$(dobdc) that showed distinctive high C_2H_6/C_2H_4 selectivity and excellent separation performance [40]. However, the heat of adsorption and the moisture sensitivity of this special material were the highest of all reported materials for C_2H_6/C_2H_4 separation, which limited its application. Although the use of C_2H_6-selective adsorbents is favorable for this separation because of low energy consumption, the lack of sufficient stability and strong binding affinity toward C_2H_6 has impeded the practical application of these materials. To the best of our knowledge, few examples exist of MOFs with good stability and the ability to efficiently remove C_2H_6 from C_2H_6/C_2H_4 mixtures. Given the high coordination number and robustness of the scaffold assembled with the highly charged metal node with the organic linkers [41–45], we hypothesized that a titanium-based MOF material with a nonpolar surface might have great potential for paraffin-selective adsorption with high stability. Therefore, we constructed and reported the adsorption separation of C_2H_6 and C_2H_4 on a titanium MOF ZSTU-1 with high stability [46]. The material showed strong binding affinity toward C_2H_6 and adsorbed a higher amount of C_2H_6 than C_2H_4, especially at low pressures. In addition, the C_2H_6 distribution simulated by the grand canonical Monte Carlo method (GCMC) also confirmed the stronger binding affinity toward C_2H_6 of this scaffold. Moreover, the dynamic breakthrough experimental results suggested that ZSTU-1 could efficiently remove C_2H_6 from C_2H_6/C_2H_4 mixtures (1:9 and 1:15, volume ratio) to afford high-purity C_2H_4 (>99.95%). Moreover, the maintained structure and unchanged sorption performance of ZSTU-1 after cycling measurements and various examinations for stability indicated that these materials have great potential for C_2H_6/C_2H_4 separation on an industrial scale.

2. Experimental

2.1. Synthesis of ZSTU-1

ZSTU-1 was synthesized according to the approach reported previously, with minor modifications. All the chemical reagents were used as received without further purification. 4,4′,4″-nitrilo tribenzoic acid (H_3TCA) (0.377 g, 1 mmol) was added to *N*,*N*-dimethylformamide (DMF, 5 ml) and fully dissolved by continuous stirring at room temperature in a 25 ml Teflon vessel. Then, 0.31 ml (1 mmol) titanium(IV) isopropoxide [$Ti(OiPr)_4$] was introduced into the mixture, and a bright yellow solution was immediately formed. Thereafter, the Teflon vessel was sealed and transferred into an autoclave maintained at 478 K for 24 h. After the mixture was naturally cooling down to the room temperature, the solution was centrifuged and washed thrice with DMF and thrice with methanol, and the desired yellow sample was obtained after drying overnight in a vacuum oven at 358 K. For gas sorption measurements, the guest-free sample was obtained after activation of the yellow powder at 393 K until no further mass loss was observed. For structural stability investigations, 0.02 g sample was soaked in 4 ml vial filled with corresponding solvent to determine the solvent and acid/base stability of ZSTU-1. For moisture stability, the 0.02 g sample was exposed to water vapor in a sealed vial containing different concentration NaCl solution. Ethane (C_2H_6, 99.99%), ethylene (C_2H_4, 99.99%), helium (He, 99.999%), nitrogen (N_2, 99.99%), and C_2H_6/C_2H_4 mixed gases (1:1, 1:9, and 1:15, volume ratio) were purchased from Beijing Special Gas Co. Ltd, China.

2.2. Characterization

Powder X-ray diffraction (PXRD) patterns were recorded on a Bruker D8 ADVANCE X-ray diffractometer by employing Cu-K_α radiation (λ = 1.5418 $\times$ 10^{-10} m) at 30 kV over the 2θ range of 5°–40° at a scanning rate of 1 (°)·min^{-1}. Further, scanning electron microscopy (SEM) was performed to observe the morphology of the sample using a Hitachi SU8010 scanning electron microscope. Thermogravimetric analysis (TGA) was conducted under N_2 conditions with a NETZSCH STA 449F5 thermal analyzer at a heating rate of 5 K·min^{-1} from room temperature to 1073 K.

2.3. Gas sorption measurements

An Intelligent Gravimetric Analyzer (IGA 001, Hiden, UK) was employed to precisely record the C_2H_4 and C_2H_6 adsorption isotherms using gravimetric techniques at equilibrium conditions. Before each experiment, the solvent-exchanged sample was degassed at high vacuum (>10^{-3} kPa) until no further mass loss was observed. The N_2 sorption isotherms of ZSTU-1 at 77 K were obtained using a Micromeritics ASAP 2020 analyzer after the sample was fully activated. The samples were activated at 393 K over 4 h to remove the guest molecules prior to each measurement.

2.4. Dynamic breakthrough experiments

The dynamic breakthrough experiments were performed using the homemade set-up composed of two columns for the separation analysis. One of the columns loaded with the activated MOF powder was used for adsorption, while the other was employed to stabilize the flow rate of the gas mixture. The flow rate at the inlet and outlet of the adsorption column was controlled simultaneously by a pressure gauge and a mass flow meter. During the experiment, the effluent gas from the adsorption column was monitored by using a gas chromatography system (GC-2014C Shimadzu) equipped with a thermal conductivity detector. For the cycling breakthrough experiments, the adsorption column was purged *in situ* with helium at a flow rate of 30 ml·min^{-1} for 30 min. All gases used were of high purity (99.99%).

2.5. Simulation methods

To evaluate the mechanism of C_2H_6-slective adsorption in the framework, GCMC simulations were performed to determine the adsorption sites of C_2H_6. These simulations were performed using the sorption module with the COMPASS force field in Materials Studio. The Lennard-Jones interactions were calculated using a cut-off radius of 12.0 $\times$ 10^{-10} m, while the Coulombic and van der Waals interactions were handled with the Ewald summation method. The MOF structure was treated as rigid with the building atoms frozen at their original crystallographic positions during the

simulations. For each state point, 2.0×10^7 steps were used to guarantee adsorption equilibrium.

3. Results and Discussion

3.1. Characterization of ZSTU-1

As shown in the Fig. 1(a), six Ti atoms were linked by the organic linkers to form the $Ti_6(\mu_3\text{-}O)_6(COO)_6$ cluster, and these Ti_6 clusters were further connected to form a 1D infinite nano-rod through the μ_2-OH groups; next, *via* the connection of six of the Ti_6 clusters, these nano-rods were extended by the TCA linkers and joined to form the 3D porous structure with 1D hexagonal channels along the *c* axis, as shown in Fig. 1(b) (depicted as the yellow hexagonal prism). This special structure was similar to that of the typical MOF-74 and MIL-177-HT [25,47] as demonstrated in Fig. S1 (in Supplementary Material). The recorded PXRD patterns of ZSTU-1 was consistent with those of the simulated one, confirming the successful synthesis and good crystallinity of the sample (Fig. S2). The morphology of this MOF was hexagonal, as seen in the SEM images in Fig. S3. TG curves showed two-step mass loss during heating: the first one might be caused by the removal of guest solvents and the —OH groups, while the second one is attributed to the disintegration of the structure. Moreover, the remained PXRD patterns at 598 K indicating the excellent thermal stability of ZSTU-1 (Fig. S4). The N_2 sorption isotherm at 77 K was used to determine the permanent porosity of ZSTU-1. As shown in Fig. S5, ZSTU-1 exhibited a microporous structure with the pore size distribution and BET surface area of 0.7×10^{-10} m and 563 $m^2 \cdot g^{-1}$ (Langmuir surface area: 1559 $m^2 \cdot g^{-1}$), respectively.

3.2. C_2H_6/C_2H_4 adsorption isotherms and selectivity of ZSTU-1

The adsorption of C_2H_6 and C_2H_4 on the prepared ZSTU-1 with 1D non-polar surface channels was investigated. The structure exhibited the inversed adsorption performance. And the amount of C_2H_6 adsorbed (26.3 $cm^3 \cdot g^{-1}$) was larger than C_2H_4 (15.8 $cm^3 \cdot g^{-1}$) especially at the low pressure 1 kPa (Fig. 2(a)) at ambient conditions; this performance is superior to that of most C_2H_6-selective adsorbents, such as ZIF-7 (0.259 $cm^3 \cdot g^{-1}$), PCN-250 (5.10 $cm^3 \cdot g^{-1}$), JNU-2 (3.67 $cm^3 \cdot g^{-1}$), and Ni(bdc)$(ted)_{0.5}$ (1.94 $cm^3 \cdot g^{-1}$) (Fig. 2b). Further, this exceptional adsorption performance encouraged us to investigate the strong binding affinity toward C_2H_6 in detail. We calculated the IAST selectivity for the C_2H_6/C_2H_4 mixture based on the dual-sites Langmuir-Freundlich fitting parameters of the adsorption isotherms (Fig. S6): the IAST selectivity in the case of the 1:1 (volume ratio) C_2H_6/C_2H_4 mixture was 2.3 at 298 K and 100 kPa. Then, the isosteric heat of adsorption for both components was determined using the Clapeyron-Clausius equation, on the basis of the virial fitting parameters for C_2H_6 and C_2H_4 adsorption isotherms recorded at 298 K, 288 K, and 273 K (Fig. S7). The obtained isosteric heat of adsorption for C_2H_6 was 43 $kJ \cdot mol^{-1}$ larger than that for C_2H_4 (32 $kJ \cdot mol^{-1}$) under the zero-coverage region, which was consistent with the adsorption isotherms (Fig. 2 (c)–(e)). Therefore, the selectivity and adsorbed amount of C_2H_6 at 1 kPa of the C_2H_6-selective adsorbents were compared, and the performance of ZSTU-1 was comparable to that of the benchmark material MAF-49 (Fig. 2(f)).

3.3. Dynamic breakthrough experiments and GCMC simulations

To further evaluate the separation performance of ZSTU-1, dynamic breakthrough experiments were carried out online using a homemade set-up (Fig. S8) for actual separation using three C_2H_6/C_2H_4 mixture compositions (1:1, 1:9, and 1:15, volume ratio). As shown in Fig. 3(a)–(c), C_2H_4 was first eluted from the adsorption column and reached the equilibrium concentration, while C_2H_6 was preferentially adsorbed and remained the adsorption column until adsorption saturation was reached. The breakthrough time intervals for the three C_2H_6/C_2H_4 mixtures were 3 min, 5 min, and 10 min, respectively; during these time intervals, C_2H_4 with a high purity could be collected directly at the outlet of the column without much energy consumption. In addition, at room temperature, the diffusion rate for C_2H_6 was higher than that for C_2H_4 (Fig. S9), and this excellent separation performance in dynamic conditions was consistent with the single component adsorption isotherms for two components. We also calculated the dynamic adsorption capacity for C_2H_6 and C_2H_4 at mixed gas condition, and their capture amounts were 34.86 $cm^3 \cdot g^{-1}$ and 24 $cm^3 \cdot g^{-1}$ for equimolar C_2H_6/C_2H_4 mixture respectively (Fig. S10). Thus, the promising applicability of ZSTU-1 in practical separation was confirmed.

To further elucidate the adsorbent's strong binding affinity toward C_2H_6, the GCMC simulations were conducted to get insight into the interactions and identify the potential adsorption sites at both 1 kPa and 100 kPa at 298 K. Fig. 4(a)–(b) shows the adsorbed C_2H_6 density distributions after the C_2H_6 molecules were introduced into the structure and adsorption equilibrium was achieved. The area for C_2H_6 adsorption at both pressures was located at the corner part adjacent to uncoordinated carbonyl oxygen of Ti-O nano-rod in the hexagon oval channels, and the adsorbed amount increased with the pressure, as indicated by the higher concentration of red dots at 100 kPa. Due to the non-planar ligands, the three

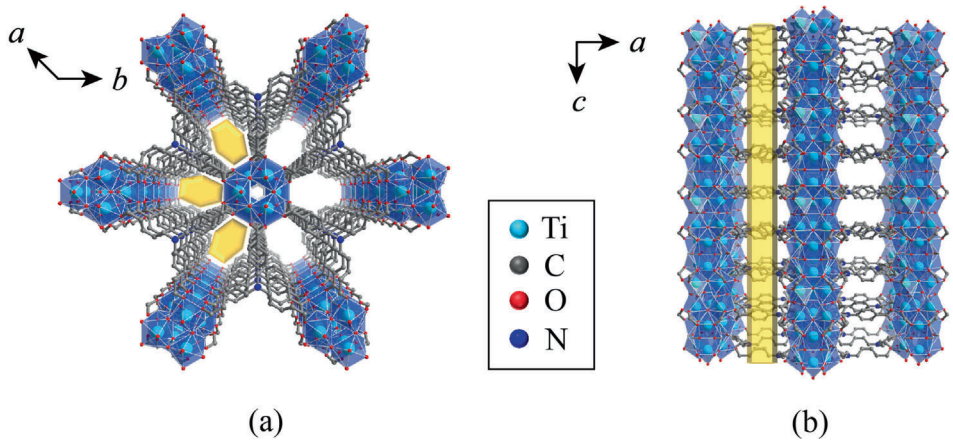

Fig. 1. A schematic illustration of ZSTU-1 synthesized for C_2H_6/C_2H_4 adsorptive separation along *c* (a) and *b* (b) direction, and hydrogen atoms were omitted for clarity.

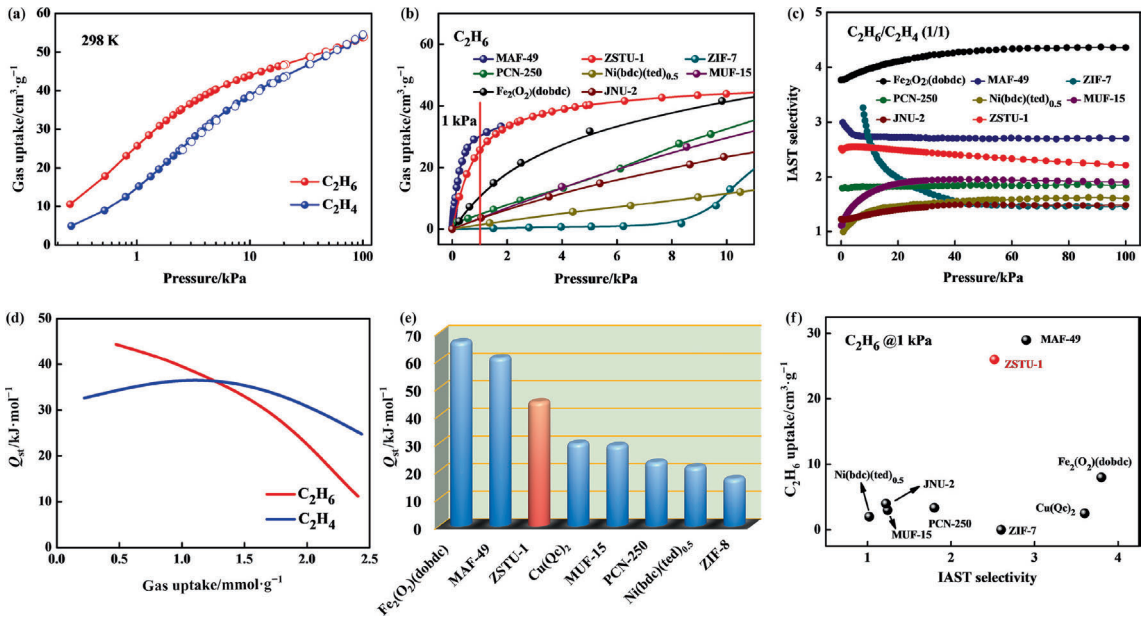

Fig. 2. C_2H_6 (red) and C_2H_4 (blue) adsorption (solid) and desorption (open) isotherms at 298 K and 100 kPa (a) and a comparison among other C_2H_6-selective adsorbents for C_2H_6 adsorption amount under low pressure at 298 K (b). IAST selectivity of ZSTU-1 for C_2H_6/C_2H_4 (1/1, volume ratio) at 298 K (c). Isosteric heat for C_2H_6 and C_2H_4 of ZSTU-1 (d)–(e). A comparison combined with the IAST selectivity (1/1, volume ratio) and C_2H_6 adsorption capacity under 298 K and 1 kPa (f).

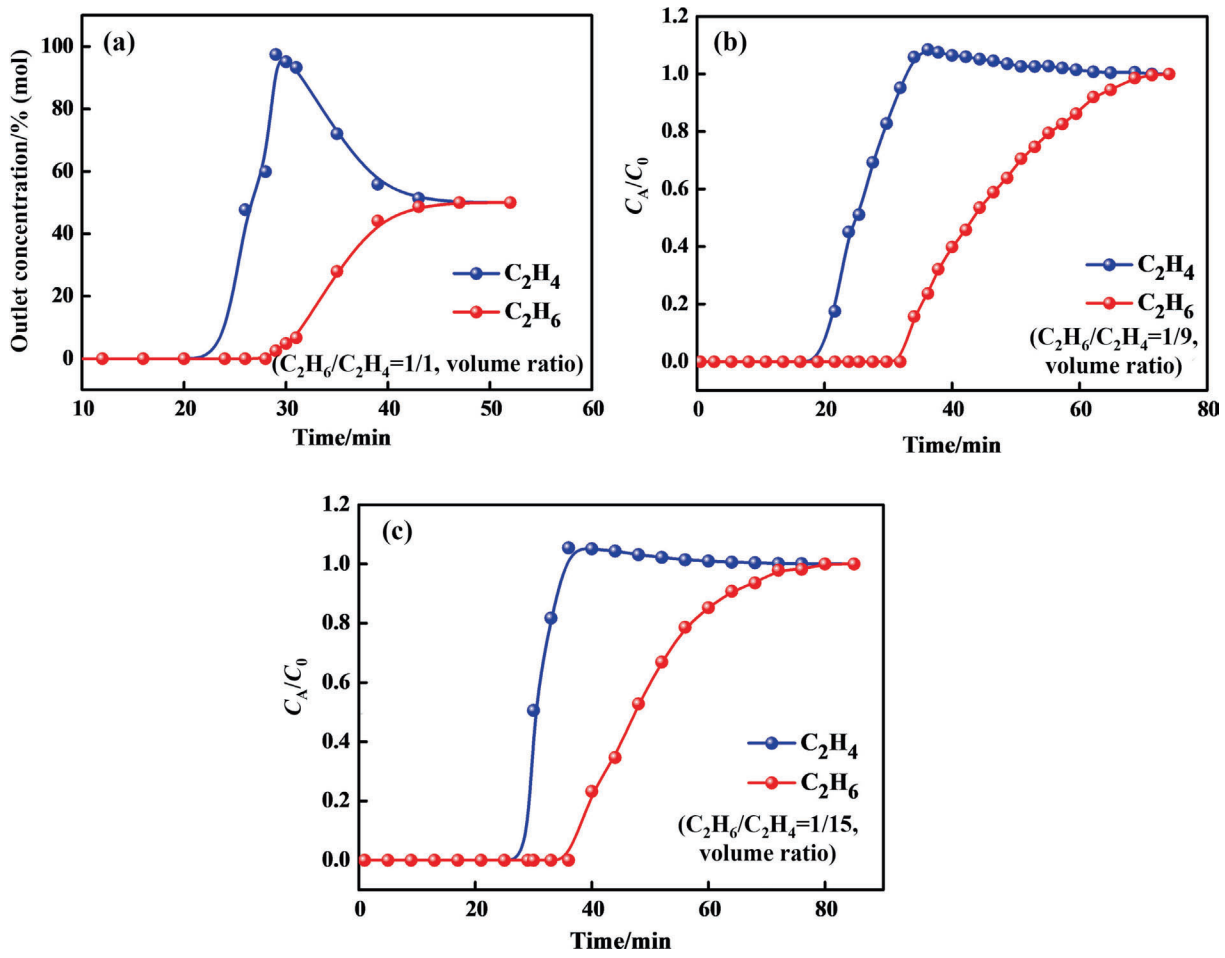

Fig. 3. Experimental breakthrough curves for 1/1 (a), 1/9 (b) and 1/15 (c) C_2H_6/C_2H_4 (volume ratio) mixture at a gas flow rate of 2.0 ml·min^{-1} at 298 K and 100 kPa.

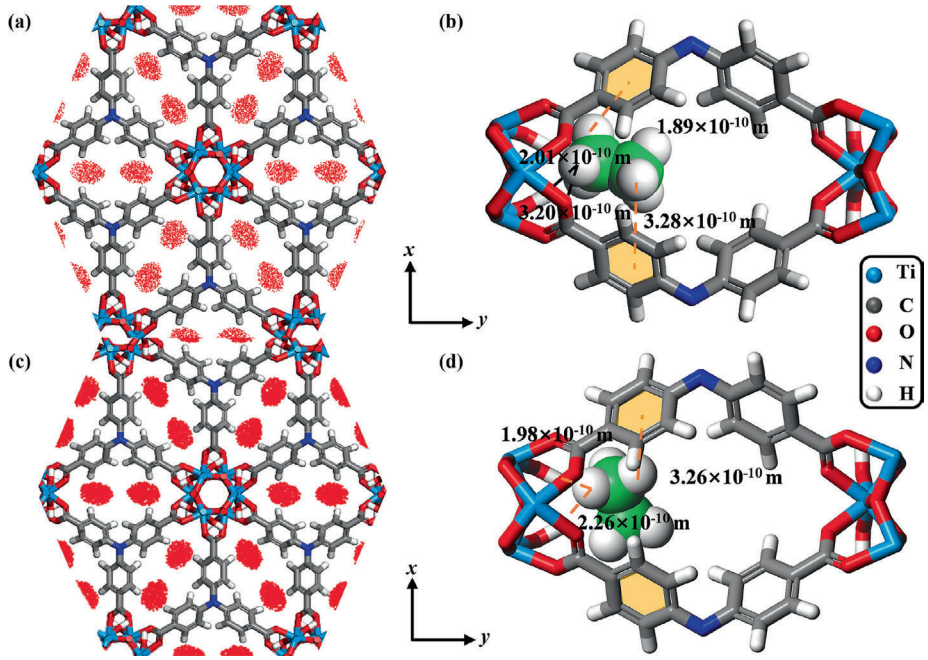

Fig. 4. The C_2H_6 adsorption distribution among the framework simulated by the GCMC method at 1 kPa (a), (b) and 100 kPa (c), (d) and 298 K respectively. (C_2H_6, red dots and green).

benzene rings rotated and formed a one-dimensional zigzag channel along the *c* axis with the non-polar surface to construct the ZSTU-1 scaffold. Furthermore, some terminal ligands like water and the —OH group grafted at the Ti—O nano-rod avoided the OMS, so the π-complexation between the unsaturated olefin and OMS would be suppressed, thus creating a suitable pore environment for C_2H_6 to be adsorbed *via* multiple hydrogen bonds and C—H···π interactions. Moreover, the measured shortest distance

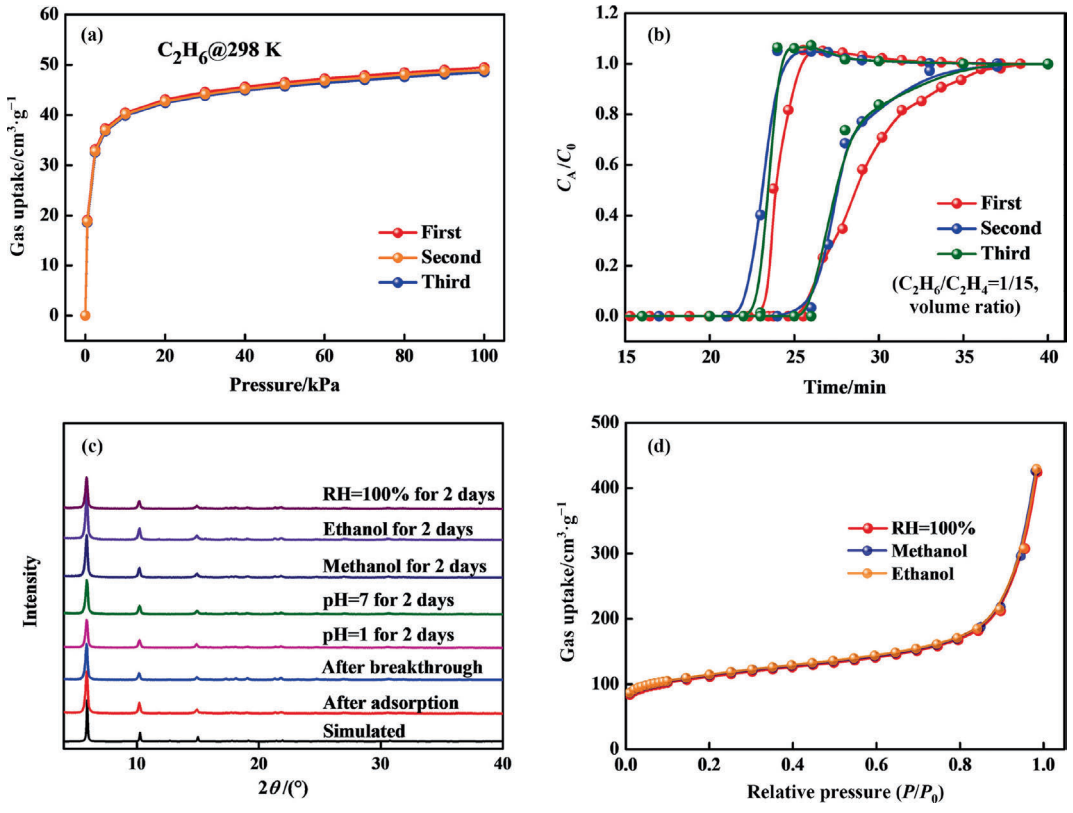

Fig. 5. Cycling adsorption isotherms for C_2H_6 and multiple breakthrough experiments for C_2H_6/C_2H_4 mixture (a)–(b). And associated PXRD patterns and N_2 sorption isotherms at 77 K showed the good structural stability of ZSTU-1 (c)–(d).

of the hydrogen bond (1.89×10^{-10} m) indicated the strong affinity between the framework and the molecules, which was in line with the calculated heat of C_2H_6 adsorption.

3.4. Structural stability investigation

The strong binding affinity toward C_2H_6 and the modest C_2H_6/C_2H_4 separation performance of ZSTU-1 encouraged us to investigate the stability of ZSTU-1 in detail. Thus, the cycling adsorption of C_2H_6 and multiple breakthrough experiments for the 1:15 (volume ratio) C_2H_6/C_2H_4 mixture were conducted at ambient conditions (Fig. 5(a)–(b)). There were no noticeable changes in the adsorption isotherms and breakthrough curves, which indicates the good cyclability of ZSTU-1. Furthermore, the intact structure was also confirmed from the PXRD patterns after adsorption and breakthrough experiments. Moreover, the moisture and solvent stability of ZSTU-1 were further explored by exposing or soaking the sample in a 4 ml sealed vial for 2 days; the PXRD pattern and almost unchanged N_2 sorption isotherms (Fig. 5(c)–(d)) confirmed the moisture stability and solvent stability of this material.

4. Conclusions

In summary, because of the lack of efficient C_2H_6-selective adsorbents with a strong binding affinity toward C_2H_6 for direct C_2H_4 purification, we constructed a titanium metal-organic framework, involving ZSTU-1 for the C_2H_6/C_2H_4 separation. The synthesized ZSTU-1 exhibited strong selective C_2H_6 adsorption over C_2H_4 in single component adsorption isotherms, especially in the low-pressure range, and this excellent performance was also validated by the results of GCMC simulations and calculation of isosteric heat of adsorption for the two components. Moreover, the conducted dynamic breakthrough experiments demonstrated that ZSTU-1 could preferentially remove trace C_2H_6 from the C_2H_6/C_2H_4 mixtures (1:9 and 1:15, volume ratio) to give C_2H_4 with a high purity in dynamic conditions. Furthermore, the distinctive good stability of this material was also confirmed *via* cycling adsorption and breakthrough experiments. This work not only presented a novel MOF for C_2H_6-selective adsorption but also paved the way for the construction of stable adsorbents with a high binding affinity toward target species.

Declaration of Competing Interest

The authors declare that they have no known competing financial interests or personal relationships that could have appeared to influence the work reported in this paper.

Acknowledgements

We gratefully acknowledge the financial support from the National Natural Science Foundation of China (21922810, 21908153, 21908155) and program of Innovative Talents of Higher Education Institutions of Shanxi. We are grateful for the supported by Cultivate Scientific Research Excellence Programs of Higher Education Institutions in Shanxi (CSREP).

Supplementary Material

Supplementary data to this article can be found online at https://doi.org/10.1016/j.cjche.2021.07.027.

References

[1] C. Zeng, Q. Hu, 2018 petroleum & chemical industry development report, *Chin. J. Chem. Eng.* 27 (10) (2019) 2606–2614.
[2] I. Amghizar, L.A. Vandewalle, K.M. van Geem, G.B. Marin, New trends in olefin production, *Engineering* 3 (2) (2017) 171–178.
[3] S. Seifzadeh Haghighi, M.R. Rahimpour, S. Raeissi, O. Dehghani, Investigation of ethylene production in naphtha thermal cracking plant in presence of steam and carbon dioxide, *Chem. Eng. J.* 228 (2013) 1158–1167.
[4] E. López, E. Heracleous, A.A. Lemonidou, D.O. Borio, Study of a multitubular fixed-bed reactor for ethylene production *via* ethane oxidative dehydrogenation, *Chem. Eng. J.* 145 (2) (2008) 308–315.
[5] P. Wattanapaphawong, P. Reubroycharoen, N. Mimura, O. Sato, A. Yamaguchi, Effect of carbon number on the production of propylene and ethylene by catalytic cracking of straight-chain alkanes over phosphorus-modified ZSM-5, *Fuel Process. Technol.* 202 (2020) 106367.
[6] R. Bruce Eldridge, Olefin/paraffin separation technology: A review, *Ind. Eng. Chem. Res.* 32 (10) (1993) 2208–2212.
[7] S. Chu, Y. Cui, N. Liu, The path towards sustainable energy, *Nat. Mater.* 16 (1) (2016) 16–22.
[8] P.Q. Liao, W.X. Zhang, J.P. Zhang, X.M. Chen, Efficient purification of ethene by an ethane-trapping metal-organic framework, *Nat. Commun.* 6 (2015) 8697.
[9] M.W. Qing, D.M. Shen, M. Bülow, M. Ling Lau, S.G. Deng, F.R. Fitch, N.O. Lemcoff, J. Semanscin, Metallo-organic molecular sieve for gas separation and purification, *Micropor. Mesopor. Mater.* 55 (2) (2002) 217–230.
[10] J.R. Li, R.J. Kuppler, H.C. Zhou, Selective gas adsorption and separation in metal-organic frameworks, *Chem. Soc. Rev.* 38 (5) (2009) 1477–1504.
[11] Y.B. He, R. Krishna, B.L. Chen, Metal–organic frameworks with potential for energy-efficient adsorptive separation of light hydrocarbons, *Energy Environ. Sci.* 5 (10) (2012) 9107.
[12] Z.B. Bao, G.G. Chang, H.B. Xing, R. Krishna, Q.L. Ren, B.L. Chen, Potential of microporous metal-organic frameworks for separation of hydrocarbon mixtures, *Energy Environ. Sci.* 9 (12) (2016) 3612–3641.
[13] L.F. Yang, S.H. Qian, X.B. Wang, X.L. Cui, B.L. Chen, H.B. Xing, Energy-efficient separation alternatives: Metal–organic frameworks and membranes for hydrocarbon separation, *Chem. Soc. Rev.* 49 (15) (2020) 5359–5406.
[14] T. He, X.J. Kong, J. Zhou, C. Zhao, K.C. Wang, X.Q. Wu, X.L. Lv, G.R. Si, J.R. Li, Z.R. Nie, A practice of reticular chemistry: Construction of a robust mesoporous palladium metal-organic framework *via* metal metathesis, *J. Am. Chem. Soc.* 143 (26) (2021) 9901–9911.
[15] R.B. Lin, L.B. Li, H.L. Zhou, H. Wu, C.H. He, S. Li, R. Krishna, J.P. Li, W. Zhou, B.L. Chen, Molecular sieving of ethylene from ethane using a rigid metal-organic framework, *Nat. Mater.* 17 (12) (2018) 1128–1133.
[16] H. Li, L.B. Li, R.B. Lin, W. Zhou, Z.J. Zhang, S.C. Xiang, B.L. Chen, Porous metal-organic frameworks for gas storage and separation: Status and challenges, *EnergyChem* 1 (1) (2019) 100006.
[17] W.G. Cui, T.L. Hu, X.H. Bu, Metal-organic framework materials for the separation and purification of light hydrocarbons, *Adv. Mater.* 32 (3) (2020) e1806445.
[18] D.S. Sholl, R.P. Lively, Seven chemical separations to change the world, *Nature* 532 (7600) (2016) 435–437.
[19] A. Mersmann, B. Fill, R. Hartmann, S. Maurer, The potential of energy saving by Gas-Phase adsorption processes, *Chem. Eng. Technol.* 23 (11) (2000) 937–944.
[20] X.Q. Wang, L.B. Li, J.F. Yang, J.P. Li, CO_2/CH_4 and CH_4/N_2 separation on isomeric metal organic frameworks, *Chin. J. Chem. Eng.* 24 (12) (2016) 1687–1694.
[21] Y.Q. Huang, Y.B. Zhang, H.B. Xing, Separation of light hydrocarbons with ionic liquids: A review, *Chin. J. Chem. Eng.* 27 (6) (2019) 1374–1382.
[22] L.B. Li, R.B. Lin, R. Krishna, X.Q. Wang, B. Li, H. Wu, J.P. Li, W. Zhou, B.L. Chen, Flexible-robust metal-organic framework for efficient removal of propyne from propylene, *J. Am. Chem. Soc.* 139 (23) (2017) 7733–7736.
[23] L.B. Li, H.M. Wen, C.H. He, R.B. Lin, R. Krishna, H. Wu, W. Zhou, J.P. Li, B. Li, B.L. Chen, A metal-organic framework with suitable pore size and specific functional sites for the removal of trace propyne from propylene, *Angew. Chem. Int. Ed.* 57 (46) (2018) 15183–15188.
[24] H. Furukawa, K.E. Cordova, M. O'Keeffe, O.M. Yaghi, The chemistry and applications of metal-organic frameworks, *Science* 341 (6149) (2013) 1230444.
[25] E.D. Bloch, W.L. Queen, R. Krishna, J.M. Zadrozny, C.M. Brown, J.R. Long, Hydrocarbon separations in a metal-organic framework with open iron(II) coordination sites, *Science* 335 (6076) (2012) 1606–1610.
[26] Y.X. Wang, S.B. Peh, D. Zhao, Alternatives to cryogenic distillation: Advanced porous materials in adsorptive light olefin/paraffin separations, *Small* 15 (25) (2019) e1900058.
[27] X.Q. Wu, J.H. Liu, T. He, P.D. Zhang, J.M. Yu, J.R. Li, Understanding how pore surface fluorination influences light hydrocarbon separation in metal-organic frameworks, *Chem. Eng. J.* 407 (2021) 127183.
[28] P.D. Zhang, X.Q. Wu, T. He, L.H. Xie, Q. Chen, J.R. Li, Selective adsorption and separation of C2 hydrocarbons in a "flexible-robust" metal-organic framework based on a guest-dependent gate-opening effect, *Chem. Commun. (Camb.)* 56 (41) (2020) 5520–5523.
[29] Z.B. Bao, J.W. Wang, Z.G. Zhang, H.B. Xing, Q.W. Yang, Y.W. Yang, H. Wu, R. Krishna, W. Zhou, B.L. Chen, Q.L. Ren, Molecular sieving of ethane from ethylene through the molecular cross-section size differentiation in gallate-based metal-organic frameworks, *Angew. Chem. Int. Ed. Engl.* 57 (49) (2018) 16020–16025.
[30] L. Yang, W. Zhou, H. Li, A. Alsalme, L.T. Jia, J.F. Yang, J.P. Li, L.B. Li, B.L. Chen, Reversed ethane/ethylene adsorption in a metal-organic framework *via* introduction of oxygen, *Chin. J. Chem. Eng.* 28 (2) (2020) 593–597.
[31] J. Pires, M.L. Pinto, V.K. Saini, Ethane selective IRMOF-8 and its significance in ethane-ethylene separation by adsorption, *ACS Appl. Mater. Interfaces* 6 (15) (2014) 12093–12099.

[32] Y.W. Chen, H.X. Wu, D. Lv, R.F. Shi, Y. Chen, Q.B. Xia, Z. Li, Highly adsorptive separation of ethane/ethylene by an ethane-selective MOF MIL-142A, *Ind. Eng. Chem. Res.* 57 (11) (2018) 4063–4069.
[33] O.T. Qazvini, R. Babarao, Z.-L. Shi, Y.-B. Zhang, S.G. Telfer, A robust ethane-trapping metal-organic framework with a high capacity for ethylene purification, *J. Am. Chem. Soc.* 141 (12) (2019) 5014–5020.
[34] H. Bux, C. Chmelik, R. Krishna, J. Caro, Ethene/ethane separation by the MOF membrane ZIF-8: Molecular correlation of permeation, adsorption, diffusion, *J. Membr. Sci.* 369 (1–2) (2011) 284–289.
[35] H. Zeng, X.J. Xie, M. Xie, Y.L. Huang, D. Luo, T. Wang, Y.F. Zhao, W.G. Lu, D. Li, Cage-interconnected metal-organic framework with tailored apertures for efficient C_2H_6/C_2H_4 separation under humid conditions, *J. Am. Chem. Soc.* 141 (51) (2019) 20390–20396.
[36] C. Gücüyener, J. van den Bergh, J. Gascon, F. Kapteijn, Ethane/ethene separation turned on its head: Selective ethane adsorption on the metal-organic framework ZIF-7 through a gate-opening mechanism, *J. Am. Chem. Soc.* 132 (50) (2010) 17704–17706.
[37] W.W. Liang, F. Xu, X. Zhou, J. Xiao, Q.B. Xia, Y.W. Li, Z. Li, Ethane selective adsorbent $Ni(bdc)(ted)_{0.5}$ with high uptake and its significance in adsorption separation of ethane and ethylene, *Chem. Eng. Sci.* 148 (2016) 275–281.
[38] Y.W. Chen, Z.W. Qiao, H.X. Wu, D. Lv, R.F. Shi, Q.B. Xia, J. Zhou, Z. Li, An ethane-trapping MOF PCN-250 for highly selective adsorption of ethane over ethylene, *Chem. Eng. Sci.* 175 (2018) 110–117.
[39] R.B. Lin, H. Wu, L.B. Li, X.L. Tang, Z.Q. Li, J.K. Gao, H. Cui, W. Zhou, B.L. Chen, Boosting ethane/ethylene separation within isoreticular ultramicroporous metal-organic frameworks, *J. Am. Chem. Soc.* 140 (40) (2018) 12940–12946.
[40] L.B. Li, R.B. Lin, R. Krishna, H. Li, S.C. Xiang, H. Wu, J.P. Li, W. Zhou, B.L. Chen, Ethane/ethylene separation in a metal-organic framework with iron-peroxo sites, *Science* 362 (6413) (2018) 443–446.
[41] S. Yuan, L. Feng, K.C. Wang, J.D. Pang, M. Bosch, C. Lollar, Y.J. Sun, J.S. Qin, X.Y. Yang, P. Zhang, Q. Wang, L.F. Zou, Y.M. Zhang, L.L. Zhang, Y. Fang, J.L. Li, H.C. Zhou, Stable metal-organic frameworks: Stable metal-organic frameworks: Design, synthesis, and applications (adv. mater. 37/2018), *Adv. Mater.* 30 (37) (2018) 1870277.
[42] A.M. Hamisu, A. Ariffin, A.C. Wibowo, Cation exchange in metal-organic frameworks (MOFs): The hard-soft acid-base (HSAB) principle appraisal, *Inorg. Chim. Acta* 511 (2020) 119801.
[43] J.J. Zhu, P.Z. Li, W.H. Guo, Y.L. Zhao, R.Q. Zou, Titanium-based metal-organic frameworks for photocatalytic applications, *Coord. Chem. Rev.* 359 (2018) 80–101.
[44] H. Assi, G. Mouchaham, N. Steunou, T. Devic, C. Serre, Titanium coordination compounds: From discrete metal complexes to metal-organic frameworks, *Chem. Soc. Rev.* 46 (11) (2017) 3431–3452.
[45] G.K. Angeli, D. Batzavali, K. Mavronasou, C. Tsangarakis, T. Stuerzer, H. Ott, P.N. Trikalitis, Remarkable structural diversity between Zr/Hf and rare-earth MOFs *via* ligand functionalization and the discovery of unique (4, 8)-c and (4, 12)-connected frameworks, *J. Am. Chem. Soc.* 142 (37) (2020) 15986–15994.
[46] C.Q. Li, H. Xu, J.K. Gao, W.N. Du, L.Q. Shangguan, X. Zhang, R.B. Lin, H. Wu, W. Zhou, X.F. Liu, J.M. Yao, B.L. Chen, Tunable titanium metal-organic frameworks with infinite 1D Ti–O rods for efficient visible-light-driven photocatalytic H_2 evolution, *J. Mater. Chem. A* 7 (19) (2019) 11928–11933.
[47] S.J. Wang, T. Kitao, N. Guillou, M. Wahiduzzaman, C. Martineau-Corcos, F. Nouar, A. Tissot, L. Binet, N. Ramsahye, S. Devautour-Vinot, S. Kitagawa, S. Seki, Y. Tsutsui, V. Briois, N. Steunou, G. Maurin, T. Uemura, C. Serre, A phase transformable ultrastable titanium-carboxylate framework for photoconduction, *Nat. Commun.* 9 (1) (2018) 1–9.